Acta Geophysica (2018) 66:1291–1301
https://doi.org/10.1007/s11600-018-0218-y

RESEARCH ARTICLE - SOLID EARTH SCIENCES

On estimating time offsets in the ambient noise correlation function caused by instrument response errors

Fang Ye[1,2] · Jun Lin[1,2] · Xiaopu Zhang[1,2] · Xiaoxue Jiang[1,2]

Received: 20 September 2017 / Accepted: 25 October 2018 / Published online: 31 October 2018

Abstract
Broadband seismic networks are becoming more intensive, generating a large amount of data in the long-term collection process. When processing the data, the researchers rely almost on instrument response files to understand the information related to the instrument. Aiming at the process of instrument response recording and instrument response correction, we identify several sources of the instrument response phase error, including pole–zero change, the causality difference in instrument correction method, and the problem of filter coefficient recording. The data time offset range from the instrument response phase error is calculated from one sample point to several seconds using the ambient noise data recorded by multiple seismic stations. With different data delays, the time offset of the noise correlation function is estimated to be 74% to 99% of the data delay time. In addition, the influence of instrument response phase error on the measurement of seismic velocity change is analyzed by using ambient noise data with pole–zero change, and the results show that the abnormal wave velocity with exceeding the standard value is exactly in the time period of the instrument response error, which indicates that the instrument response error affects the study of seismology.

Keywords Time offset · Instrument response · Seismic ambient noise · Seismic velocity change

Introduction

Over the past decade, a wide range of broadband seismic networks with multiple scales and perfect seismic data centers have been established worldwide. The observation data provided by them have driven great progress in both theory and practice in seismic ambient noise research (Weaver and Lobkis 2001; Derode et al. 2003; Snieder 2004; Paul et al. 2005; Sato 2013), and this has achieved fruitful results (Campillo and Paul 2003; Shapiro and Campillo 2004; Shapiro et al. 2005; Brenguier et al. 2008a, b). The method of ambient noise cross-correlation is free from the seismological limitations of the temporal and spatial distribution of earthquakes. With the extensive development of research on the internal structure of the earth, more intensive broadband seismic networks are continuously established. More comprehensive broadband seismic networks are being established, and many new broadband seismic instruments are gradually emerging.

Most major seismic data centers, such as IRIS DMC (the Incorporated Research Institutions for Seismology Data Management Center), distribute seismic data in SEED (Standard for the Exchange of Earthquake Data) format. The SEED format provides the possibility to distribute comprehensive metadata on instrument response and seismic records. Seismologists obtain data from the data centers and then follow the instrument response correction to obtain ground motion from these original records through extensive application of standardized and simplified software for end users. In fact, they can only rely on the instrument response file and do not know the actual working status of seismic instrument, and incorrect data processing results will occur when the actual situation of the instrument is inconsistent with the record file. This is also the important reason that affects the data quality of the early broadband seismic network.

The previous studies have shown that clock synchronization errors between two stations can lead to a time offset in the noise cross-correlation function (Sens-Schönfelder 2008;

✉ Jun Lin
lin_jun@jlu.edu.cn

[1] College of Instrumentation & Electrical Engineering, Jilin University, Changchun 130026, China

[2] National Geophysical Exploration Instrument Engineering Technology Research Center, Changchun 130026, China

Xia et al. 2015; Gouédard et al. 2014). From another point of view, we analyze the causes of the phase error of the instrument response after understanding the instrument response of the broadband seismic station. The ambient noise data of the regional broadband seismic network are then used to calculate the data delays that the phase errors may cause, and further estimate the time offset range of these data delays to noise cross-correlation function which is further calculated. Finally, we discuss the influence of the time offset generated by the instrument response error on monitoring temporal variations in crustal properties.

Theory

The cross-correlation of ambient noise data recorded by A and B at two stations is given by

$$C_{AB}(t) = \int_0^T f_A(r_1, \tau) f_B(r_2, \tau + t) \mathrm{d}\tau, \tag{1}$$

where $\upsilon_A(r_1, \tau)$ and $\upsilon_B(r_2, \tau)$ are the observed fields at spatial locations r_1 and r_2, respectively, T is the observation time, τ is time, and t is the delay time. For a spatially uniform broadband noise distribution in a uniform medium with sound speed c, it can be considered (Sabra et al. 2005) that the derivative of the noise cross-correlation C_{AB} is

$$\frac{\mathrm{d}C_{AB}}{dt} \approx -\frac{\delta(t + L/c)}{L} + \frac{\delta(t - L/c)}{L}, \tag{2}$$

where the interstation distance is $L = |r_2 - r_1|$, and C_{AB} is zero for $|t| > L/c$, noncontinuous at $t = \pm L/c$, and continuous for $|t| < L/c$. The noise events that propagate from station A to B yield a positive correlation time delay t, and noise events that propagate from station B to A yield a negative correlation time delay $-t$.

It is assumed (Hannemann et al. 2014) that a delta impulse excited at time τ_δ and location r_δ in a homogeneous half-space with velocity c, which is received by station n at location r_n.

$$f_n(\tau) = \delta\left(\tau - \tau_\delta - \frac{r_n - r_\delta}{c}\right). \tag{3}$$

Similarly, when considering stations A and B and assuming that there is time delay τ_c in station B, the nonzero of the cross-correlation function of the two stations is

$$t = -\frac{L}{c} - \tau_c. \tag{4}$$

Therefore, compared with Eq. 2, the lag time of the cross-correlation function is delayed by the time τ_c, which also indicates a time delay in one of the two stations would make a time shift of the whole cross-correlation waveform to lead to a larger travel time in the positive time and a smaller travel time in the negative, or vice versa.

In practice, in addition to instrumental errors, the travel time of the surface waves for both positive and negative cross-correlation times is also affected by a physical change in the medium and a change in the spatial distribution of the noise sources (Stehly et al. 2007). So the travel time variation $\delta\tau(t)$ measured from a surface wave by cross-correlations can be written as:

$$\delta\tau(t) = D(t) + \varphi(t) + \varepsilon(t), \tag{5}$$

where $\delta\tau(t)$ is the variation in surface wave travel time measured either on the positive or on the negative part, $D(t)$ is the time delay caused by the instrumental errors, $\varphi(t)$ is the time offset due to changes in the medium, and $\varepsilon(t)$ is the time offset changes in the spatial distribution of the noise sources. $D(t)$ is an even function, and $\varphi(t)$ is an odd function.

Then, the time offset due to the station instrumental errors can be obtained from Eq 5:

$$D(t) = \frac{\delta\tau(t) + \delta\tau(-t)}{2} + \frac{\varepsilon(t) + \varepsilon(-t)}{2}, \tag{6}$$

under the assumption that $D(t)$ is large compared to $\varepsilon(t) + \varepsilon(-t)/2$, $D(t)$ can be evaluated by

$$D(t) = \frac{\delta\tau(t) + \delta\tau(-t)}{2}. \tag{7}$$

by using cross-correlation of a larger time windows, the term $\varepsilon(t)$ is expected to be smaller, and smaller long-term instrumental errors can be identified more easily.

Data and processing

With the more intensive deployment of the broadband seismic network, the development of the regional seismological network which is conducive to the study of diversified seismology is more common. Therefore, we choose the regional seismic network as the research target and select the station of the Caltech (CI) regional seismic network in the Los Angeles basin in southern California. So far, the observation data of stations in this area have been widely used in the research of ambient noise (e.g., Sabra et al. 2005; Stehly et al. 2006; Moschetti et al. 2007; Meier et al. 2010). We choose continuous data recorded from 18 stations in CI network from January 2005 to December 2006. The two-year observation window is long enough to capture the effects of seasonal variations. The distribution of the selected stations is shown in Fig. 1. The interstation distance is the key factor that determines the period range: When the interstation distance becomes much larger than the dominant wavelength, correlation in the time domain is useful (Chávez-García

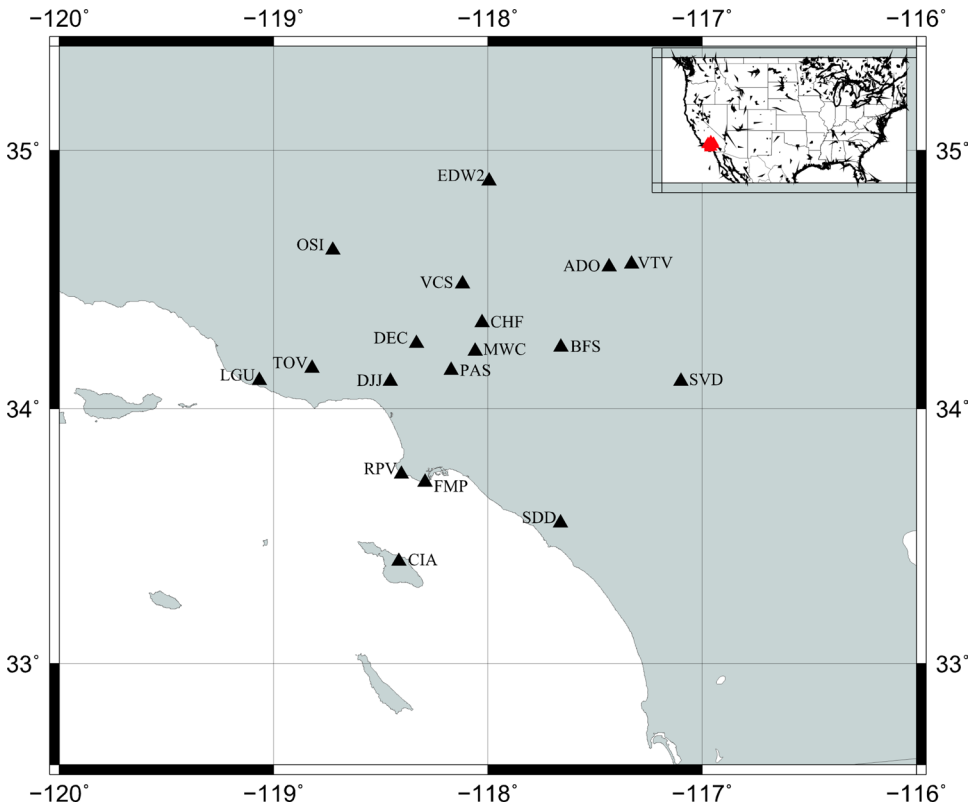

Fig. 1 Map of the study area. Stations equipped with broadband seismic instrumentation are indicated by triangles with station names beside each symbol. The inset shows the locations of stations on the larger map

and Rodríguez, 2007). All of the interstation distances are approximately 10–200 km, so the period range selected is 5–25 s. These stations are equipped with STS2 or Trillium 240 seismometers and Quanterra Q330HR digitizers, which provide mostly complete information on the nature of ground motion.

We download the SEED volumes that contain data and instrument responses from IRIS DMC. The volumes are segmented into day-long time series and resampled to 20 Hz, with mean, trend, and instrument responses subsequently removed. Therefore, we use Welch's method (Seats et al. 2012) and spectral normalization (Bensen et al. 2007) to mitigate the effects of temporal fluctuations of noise sources and to minimize the influence of high-amplitude events and instrument irregularities. After the Butterworth bandpass filtering between 5 and 25 s, the processed one-day-long traces are split into 3600 s with 50% overlap between adjacent windows. The corresponding time windows of two stations are calculated by cross-correlation, and the average of these cross-correlation results across all time windows in a single day is the 'one-day cross-correlation function.'

In order to improve the signal-to-noise ratio of the correlation trace, but also to maintain individual differences, 1-day cross-correlation functions are stacked to create daily cross-correlation functions in a moving 15-day window. Figure 2 shows daily correlation functions of the station pair DEC–TOV vary with day. High signal-to-noise ratio and similar waveforms ensure reliable estimates of temporal variations. The normalized daily cross-correlation functions present stable surface waves throughout the one year. Asymmetry of the positive and negative parts of the correlation trace is related to the nonisotropic distribution of noise sources (Stehly et al. 2006).

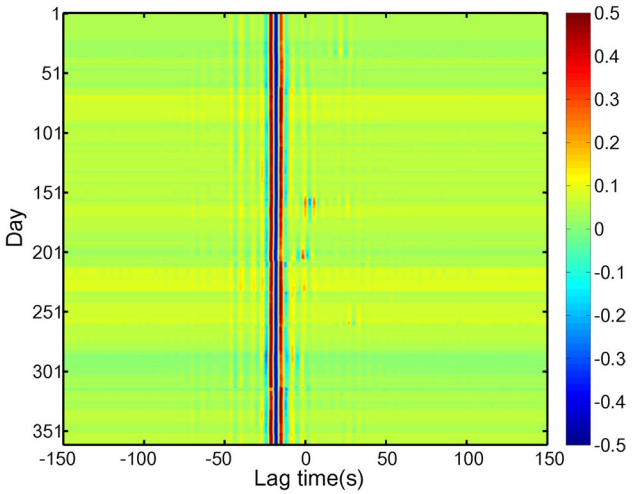

Fig. 2 Example of daily cross-correlation functions stacked using a moving 15-day window over one year at station pair DEC–TOV. The amplitude is normalized to the maximum of each correlation trace

Instrument response and sources of phase errors

Broadband seismic stations can record the complete ground motion information in the 0.01-Hz to 50-Hz frequency band, which contributes to the study of key issues such as high-resolution images of the earth's interior, evolution of the continental structure, the nature of the seismic faults, and the origin of the earthquake. We use the typical broadband seismic station in USArray's Transportable Array as an example to illustrate the configuration and deployment of broadband seismic stations, as shown in Fig. 3.

In order to obtain good low-frequency performance, the seismic station deployment needs to comply with strict installation requirements. The installation site of a broadband seismograph requires a good control environment, and other noise disturbances, such as traffic and wind noise, must be considered. To reduce interference from surface vibrations and to protect the equipment, the seismometer would be buried 10 to 20 feet below the ground inside an augered hole. This hole will be cased in either PVC or steel, to keep the hole open, and then capped to protect the hole. Power is provided by solar panels mounted nearby on a pole or a hut and powered by a combination of battery and fuel cell systems. A fiberglass hut with solar panels on the roof is placed about 3.5 m (~ 10 ft) from the sensor to house the batteries, data collection computer, and communication electronics. Cables contained within a conduit connect the sensor to the equipment in the hut. Data are transmitted to the data processing center via cellular, broadband, or satellite communication systems.

The complete broadband measurement system (sensors and data loggers) is considered as a linear time invariant (LTI) system that transfers analog input signals $x(t)$ to discrete output signals $r[t]$. In Fig. 3, a typical measurement system is displayed via the broadband high-gain vertical channel of the station TOV.

An LTI system can be described as the frequency response function of a measurement system in the frequency domain. It can be divided into three stages: analogue, analogue–digital (A/D) converter, and digital. In fact, by multiplying the discrete frequency response function at all stages, the complete frequency response function is finally obtained (Davis et al. 2005):

$$G(f) = S_d A_0 \frac{\prod_{n=1}^{N}(s - r_n)}{\prod_{m=1}^{M}(s - p_m)} = S_d A_0 H_p(s), \tag{8}$$

where the scalar S_d contains all information about the stage's sensitivity, the factor A_0 is chosen to normalize the series at a canonical frequency f_0, r_n and p_m are the zeros and poles. The variables in the Laplace transform are given by s which related to angular frequency via the $s = i\omega$.

In addition, oversampling is commonly used to reduce the quantization noise of A/D converter and improve amplitude resolution. Then, the original discrete data stream $x[t]$ is low-pass filtered and resampled to obtain the expected sampling rate of the discrete time series $r[t]$. In general, the

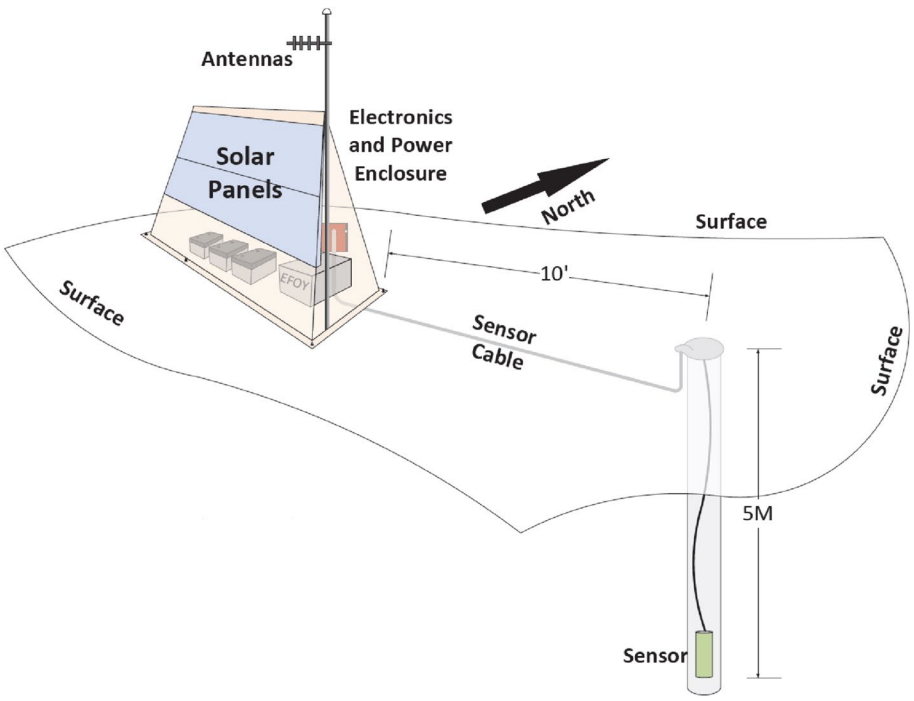

Fig. 3 Schematic diagram of the configuration of a typical broadband seismic station

sampling to the desired sampling rate is obtained by cascading a number of extractors with digital anti-alias (DAA) filters, as shown in Fig. 4.

The SEED format provides all the analog phase, digital stage instrument response information and also includes the transfer function of the DAA filter stage. The discrete transfer function T(z) of the DAA filter in the digital z plane is usually described by the numerator and denominator coefficients:

$$T(z) = \frac{\sum_{l=0}^{M} b_l z^{-l}}{\sum_{k=0}^{N} a_k z^{-k}}. \quad (9)$$

In general, the data acquisition system can program the DAA filter with a minimum phase filter or a linear phase filter and also correct the delay generated by the linear phase filter.

Moreover, the broadband sensor needs special attention because it has a high sensitivity to low-frequency interference caused by temperature-induced tilt. In some cases, it may even be necessary to install it in the borehole to keep away from the noise near the surface. The vertical sensor is affected by variable buoyancy caused by pressure changes. In short, each instrument will provide response parameters accurately in layout, but with a long time of work, they may be aging or other deviations, so the actual response parameters of the instrument need to be regularly measured and modified.

In the process of seismic data processing, the instrument information is only involved in deconvolution operation with the form of instrumental response of Eq. 8. Therefore, the phase error of instrument response is mainly generated in the process of instrument response recording and instrument response correction. We analyze several sources of error in this process, including the change of the pole–zeros related to the phase of the instrument response in Eq. 8, the error in the record of the transfer function coefficient of the DAA filter in Eq. 9, and the causality difference in different instrument response correction methods.

The change of pole–zeros

During a long period of data collection, the replacement or aging of the broadband sensor may cause the actual pole–zeros to deviate from the recorded pole–zeros. Besides, atmospheric pressure, humidity, and temperature may also cause the change of pole–zeros. If it is not timely to measure the new pole–zeros and update the instrument response file, but using the pole–zeros recorded in the original instrument response file for data processing, it is possible to cause the time offset of the noise cross-correlation function.

We take station TOV as an example, and its pole–zeros due to the replacement of the seismograph have changed as shown in Fig. 5. The two instrument responses before and after the pole–zero change are calculated according to Eq. 8, and they are used in the instrumental correction for one-day ambient noise data of the station TOV. The time difference between the two groups of noise data after instrumental correction is 0.025 s in period band 5–10 s and 0.063 s in period band 10–25 s, respectively.

The problem of transfer function coefficients

The SEED format records the coefficients of the transfer function of the DAA filter stage according to Eq. 9 and the correction time of the linear phase filter. The delay time of the filter means that the data move backwards through the filter, and then the data logger corrects the time series by shifting the time series back to the earlier time after filtering. The usual instrumental correction is based on Eq. 8, so the time delay that has been corrected in the acquisition system is not considered. However, when the recorded filter coefficients differ from the actual corrected time delay, there will be a delay in the recording data.

We use a common mistake as an example to illustrate that the coefficients are recorded in reverse order; in fact, SEED format specifies that the coefficients should be recorded in the forward order. The filter with the inverse coefficient has the same amplitude response spectrum as the original filter, but has a distinct phase response spectrum, so there will be a different time delay. The filter coefficients recorded in the instrument response file of station CIA are calculated in two different orders, as shown in Table 1, which contains delay times calculated by filter coefficients in forward order,

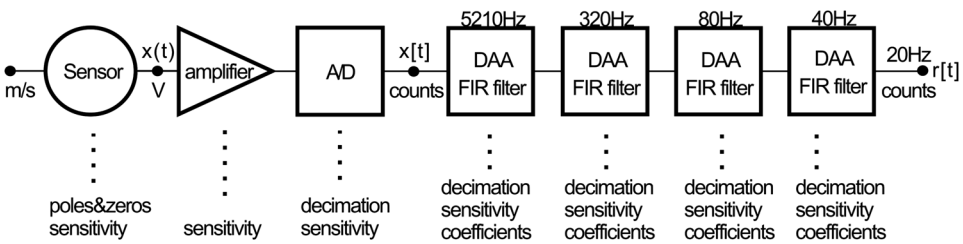

Fig. 4 Block diagram of the broadband high-gain vertical channel of a seismological measuring system sampling at 20 Hz. The description of the corresponding instrument response in the SEED is marked below each part

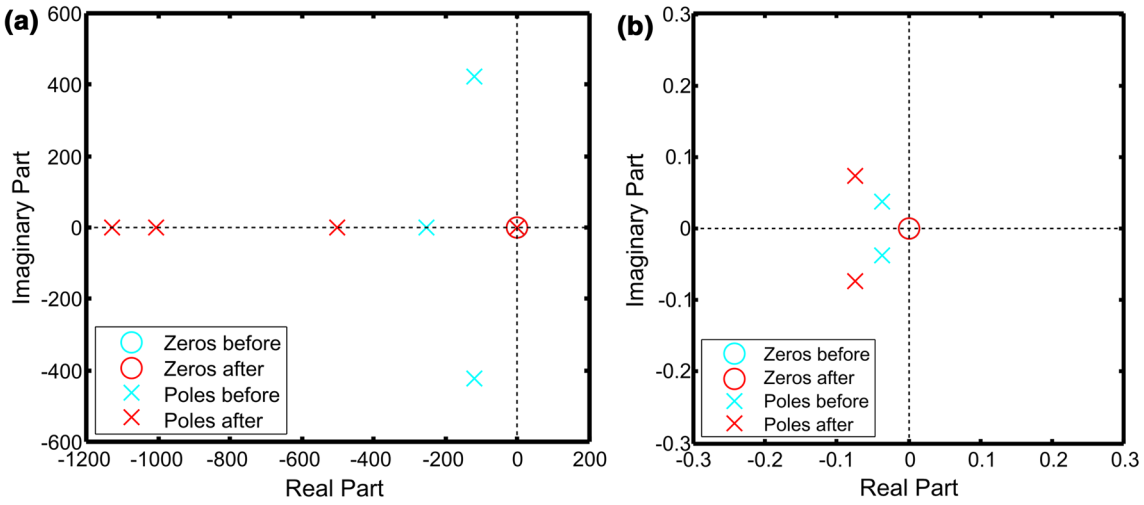

Fig. 5 **a** Pole–zeros of station TOV are distributed before and after the change. **b** Zoom-in coordinates near 0 point in (**a**)

Table 1 Delay times of filters in station CIA

Different conditions	Stage 4 (s)	Stage 5 (s)	Stage 6 (s)	Total delay time (s)
Filter in forward order	0.003	0.012	0.398	0.413
Correction time	0.003	0.012	0.398	0.413
Filter in reverse order	0.024	0.276	0.852	1.152
Difference	0.021	0.264	0.464	0.739

correction times in the data logger, delay times calculated by filter coefficients in reverse order, and the delay time differences between the two kinds of coefficients. With the decreasing sampling rate at each stage, the delay time difference caused by the coefficient order becomes larger. For low sampling data, such mistakes would lead to greater errors, and the time delay difference is significantly up to 0.464 s in the stage 6. The total delay time difference in all stages is 0.739 s, which is different from the correction time, resulting in the time offset of data.

The causality of instrumental correction

Haney et al. (2012) described a general method for causal instrumental correction, with particular attention to maintaining causal properties after correction in order to observe the first action and maintain relative timing information between different frequencies. However, most of the instrumental response correction methods are noncausal. The causality of instrumental correction mainly lies in the choice of filter, so we compare the zero-phase filters commonly used in instrumental correction with IIR causal filters used in causal instrumental correction. Then, the two instrumental correction methods are, respectively, used for one day of ambient noise raw data from station SDD, and the time difference between the two corrected data is 0.03 s.

Time offset measurement results

We have made clear that the instrument itself, the data processing, and the management of the metadata are several sources that may cause the phase error of the instrument response in the process of long-time data acquisition. In order to understand the influence of these errors on the data, the time offset caused by the phase error of the instrument response is calculated by using the ambient noise data of the 18 seismic stations shown in Fig. 1.

During the 2-year observation period, only station TOV has pole–zero change. Therefore, in order to explain the time offset caused by different pole–zero changes, there is also a station CHF for selected longer observation (4 years). The instrumental response of two stations before and after the pole–zero changes is calculated, respectively, and the phase frequency characteristic curves of the two stations are obtained, as shown in Fig. 6.

The phase of the instrument response of the two stations increases gradually from short period to long period: one station reached 10 degrees and the other 20 degrees in the

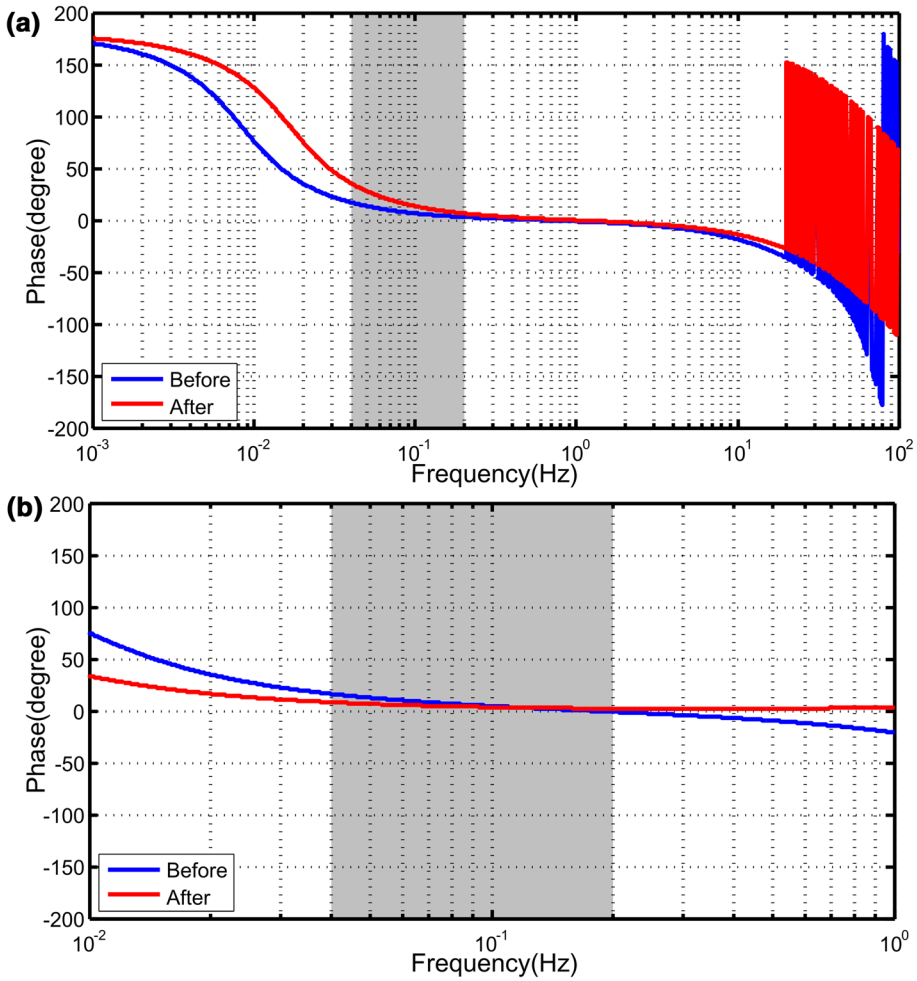

Fig. 6 Phases of the instrument response of (**a**) the station TOV and (**b**) the station CHF are calculated from the pole–zeros before and after the change. The frequency band we are working with is indicated by gray shading

Table 2 Average time offset caused by the change of pole–zeros

Station	Time offset in period 5–10 (s)	Time offset in period 10–20 (s)
CHF	−0.0313	−0.0375
TOV	−0.0500	−0.1375

frequency range we studied, suggesting that the time offset caused by the change of pole–zeros is frequency dependent. Therefore, we choose the two-band range of 5–10 s and 10–20 s, respectively, and the two instrument responses before and after the pole–zero change of each station are used to for instrumental correction of a day series. The time offset between the two datasets per day was repeated over the two-year observation, and the average time offset is shown in Table 2.

The result of time offset is related to the frequency dependence of the phase, in which the phase change of the CHF station is smaller than that of the station TOV, so its time offset difference is also smaller within two periods. This verifies that the pole–zeros of the seismograph are changed if updates to the instrument response file are not made in time, which can introduce unnecessary data delay.

We have known that the time offset of a single day's time series of station SDD caused by causality differences in instrumental correction is 0.03 s. For each of the 18 stations, the time shift of each day in the observation is calculated and the average time offset caused by the causality differences in the instrumental correction is finally obtained as shown in Table 3. The time offset caused by this error is about 2 sampling points, but it is an error that cannot be ignored in the study of seismology, such as the clock synchronization of an underwater geophone, which requires accurate time values.

The transfer function coefficient record problem or the correction time error of data acquisition system will lead to the time offset of data time series. We consider calculating the time offset of data from all 18 stations caused by this error, in which the filters of the station ADO are the same as those of the stations BFS, CHF, FMP, RPV, SDD, SVC, the filters of the station CIA are the same as those of the stations DJJ, LGU, MWC, SDD, VCS, and the filters of the station OSI are the same as those of the stations PAS, SVD, TOV,

Table 3 Average time offset caused by causality differences

Station	Time offset (s)
ADO	−0.0391
BFS	−0.0333
CHF	−0.0250
CIA	−0.0362
DEC	−0.0249
DJJ	−0.0348
EDW2	−0.0277
FMP	−0.0588
LGU	−0.0393
MWC	−0.0423
OSI	−0.0399
PAS	−0.0250
RPV	−0.0283
SDD	−0.0252
SVD	−0.0262
TOV	−0.0465
VCS	−0.0234
VTV	−0.0334

VTV. Therefore, the data time offset caused by the transfer function coefficients of two different orders is calculated by selecting the filter of ADO, CIA, and OSI, and the results are shown in Table 4. If an incorrect instrument response is used to recover ground motion from the data record, the time series is likely to exceed the time offset of 1 s in this error case.

In particular, the result of these errors is to delay or advance the time series of the ambient noise, so we analyze the effect of the time offset caused by the phase error of the instrument response on the time offset of the noise cross-correlation function. The data of the station ADO are selected as the target, and the data time offset of the station ADO is about 1 s due to the transfer function coefficient problem, so the one-day sequence after the background noise data preprocessing is delayed about 1 s. And from the previous results, it is known that the time offset of the data generated by the instrument response error ranges from a sampling point to a few seconds, so different data time offsets (0.05 s, 0.1 s, 0.5 s, 1 s) are set up to represent the results of different instrument response phase error sources.

Table 4 Time offset caused by the problem of transfer function coefficients

Station	Stage 4 (s)	Stage 5 (s)	Stage 6 (s)	Sum (s)
ADO	0.026	0.243	0.496	0.765
CIA	0.021	0.264	0.454	0.739
OSI	0.067	0.418	0.641	1.126

The interstation distance between ADO and VTV is only 9.6 km and does not satisfy the condition of building a noise cross-correlation function. Therefore, data from ADO and the other 16 stations are used to calculate the travel time offset $\delta\tau(t)$ between the daily cross-correlation functions obtained from the time offset data and the daily cross-correlation functions obtained from the original data and to obtain the time offset $D(t)$ of noise cross-correlation function caused by phase errors in instrument response according to Eq. 7. Finally, we obtain the average time offset of the cross-correlation function of all station pairs during the observation, as shown in Table 5.

The effect of the noise source on the each of the two cross-correlation functions is the same, so the time offset obtained is only influenced by the time error of the instrument. From the results, with the increase in delay time, the time offset of noise cross-correlation function increases. The results measured in the period band of 10–20 s are less than 5–10 s. In spite of the minimum delay time, the time offset also reaches 74% of the delay time. Although we simulate the data delay caused by the instrument response error, it can be seen that the phase error of the instrument will cause an obvious time offset of noise cross-correlation function, which will affect the study of surface wave imaging (Shapiro et al. 2005; Sabra et al. 2005; Lin et al. 2007), wave velocity monitoring (Wegler and Sens-Schönfelder 2007; Brenguier et al. 2011; Durand et al. 2011), and ground motion prediction (Prieto and Beroza 2008; Denolle et al. 2013, 2014) using the noise cross-correlation function in seismology.

Application of monitoring velocity variations

Ambient noise interferometry has widely been applied in monitoring temporal variations in crustal properties in recent years (Sens-schönfelder and Wegler 2006; Wegler and Sens-schönfelder 2007; Brenguier et al. 2008b). Because ambient noise is recorded at all times and places, the passive monitoring method is more repeatable and avoids the uncertainty in earthquake source locations and origin times and also more economical than controlled repeated sources.

Table 5 Average time offset of noise cross-correlation functions of all station pairs

Data delay time (s)	D(t) in 5–10 (s)	ΔD(t) in 5–10 (s)	D(t) in 10–20 (s)	ΔD(t) in 10–20 (s) (%)
0.05	−0.0422	84%	−0.0368	74
0.1	−0.0906	90%	−0.0781	78
0.5	−0.4898	98%	−0.4758	95
1	−0.9898	99%	−0.9758	98

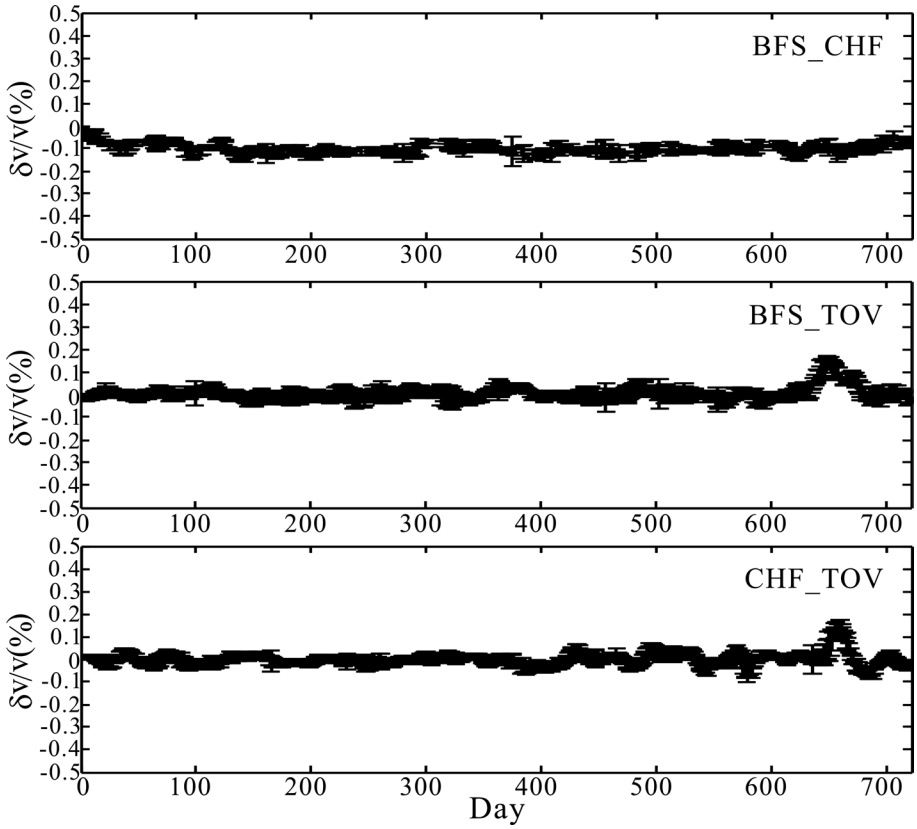

Fig. 7 Temporal velocity perturbations and errors at three station pairs: **a** BFS–CHF, **b** BFS–TOV, and **c** CHF–TOV

Therefore, it enables continuous monitoring the temporal evolution of the seismic wave velocity of the medium by tracking the time shifts of noise cross-correlation function.

If the medium experiences a spatially homogeneous relative seismic velocity change $\Delta v/v$, the relative travel time shift $\Delta\tau/\tau$ between a short-term current Green function and the long-term reference Green function is independent of the lapse time at which it is measured and $\Delta v/v = -\Delta\tau/\tau$. We followed the optimization method of Brenguier et al. (2008a, b) using the moving window cross-spectral analysis to monitor variations in seismic velocity. In a short window centered at time τ, there are cross-spectrum between the reference correlation function and the current correlation function, and phase difference between the two traces in different frequency. If the two waveforms are similar, the time difference between the two traces $\Delta\tau$ is estimated by the slope of phase differences $\Delta\tau = \Delta f/(2\pi \times f)$. Then, the linear fitting slope of the time offset calculated in a series of continuous narrow windows over a path between the two stations is the negative of the average fractional velocity perturbation, i.e., $\Delta\tau/\tau = -\Delta v/v$.

We choose the noise cross-correlation function of the station pairs composed of three stations BFS, CHF, and TOV. Among them, the pole–zeros of the instrument response at station TOV were changed on day 644 as shown in Fig. 1. We have shown that failure to update the instrument response file in time will result in data delay and time offset of the noise correlation function. Therefore, the original instrument response file is selected for the instrument response correction of the station TOV in data preprocessing to simulate this error. For each station pair, the noise cross-correlation functions stacked over the 2-year period of study define the long-term reference trace and the noise cross-correlation functions stacked in 15-day-long moving windows defines the short-term current Green function.

Figure 7 presents the relative velocity changes $\Delta v/v$ measured over 2 years for the three station pairs, and the seismic velocity variations are small ($< \pm 0.1\%$). The station pairs BFS–TOV and CHF–TOV yield similar temporal variations which reveal a prominent sudden increase in seismic velocity perturbation of ~ 0.2% about on day 650, after this increase, the velocity gradually returns to its mean level. Because three stations are in the same area, the changes in the geological structure will result in all three station pairs to have seismic velocity perturbations at the same time. Therefore, only the stations connected with the TOV station have the speed disturbance, which is consistent with the expected station TOV, indicating the influence of the instrument response error on the geological structure study. Therefore, only the station pairs related to the station TOV have the velocity disturbance, which is consistent with the expected instrument response error of the station TOV, indicating the

influence of the instrument response error on analyses of changes in geologic structure.

Conclusion

On the basis of understanding the configuration of the broadband seismograph, the calculation of the instrument response, and the parameters of the corresponding SEED format metadata, we analyze several sources of the instrument response phase error, including the change of the pole–zeros, the problem of the parameter recording of the filter transfer function, and the causality difference in different the instrument response correction methods. Using the ambient noise data of 18 broadband seismic stations, the time offset of the data caused by the three phase error sources is calculated from one sampling point to a few seconds. By setting the data time delay of the station ADO caused by instrument response error which is 0.05 s, 0.1 s, 0.5 s, and 1 s, we obtain time offset range of the noise cross-correlation function which is 74% to 99% of data delay time. Therefore, we demonstrate that the time offset of noise cross-correlation function is not only related to clock synchronization, but also closely related to instrument response. In addition, we use ambient noise data with instrument response phase error and the method of ambient noise seismic interferometry, to analyze the influence of the instrument's phase error data on the relative variation in wave velocity. The results show that when monitoring the relative changes in seismic wave velocity, disturbances significantly larger than standard wave velocity occur during instrument response errors that experience pole–zero changes. The stability of instrument response and the accuracy of processing are prerequisites for data analysis, especially for ambient noise data.

References

Bensen GD et al (2007) Processing seismic ambient noise data to obtain reliable broad-band surface wave dispersion measurements. Geophys J Int 169:1239–1260. https://doi.org/10.1111/j.1365-246X.2007.03374.x

Brenguier F, Campillo M, Hadziioannou C, Shapiro NM, Nadeau RM, Larose E (2008a) Postseismic relaxation along the San Andreas Fault at Parkfield from continuous seismological observations. Science 321:1478–1481. https://doi.org/10.1126/science.1160943

Brenguier F, Shapiro NM, Campillo M, Ferrazzini V, Duputel Z, Coutant O, Nercessian A (2008b) Towards forecasting volcanic eruptions using seismic noise. Nat Geosci 1:126–130

Brenguier F, Clarke D, Aoki Y, Shapiro NM, Campillo M, Ferrazzini V (2011) Monitoring volcanoes using seismic noise correlations. Comptes Rendus Geosci 343:633–638

Campillo M, Paul A (2003) Long-range correlations in the diffuse seismic coda. Science 299:547–549. https://doi.org/10.1126/science.1078551

Chávez-García FJ, Rodríguez M (2007) The correlation of microtremors: empirical limits and relations between results in frequency and time domains. Geophys J Int 171:657–664. https://doi.org/10.1111/j.1365-246X.2007.03529.x

Davis P, Ishii M, Masters G (2005) An assessment of the accuracy of GSN sensor response information. Seismol Res Lett 76:678–683. https://doi.org/10.1785/gssrl.76.6.678

Denolle MA, Dunham EM, Prieto GA, Beroza GC (2013) Ground motion prediction of realistic earthquake sources using the ambient seismic field. J Geophys Res Solid Earth 118:2102–2118

Denolle MA, Dunham EM, Prieto GA, Beroza GC (2014) Strong ground motion prediction using virtual earthquakes. Science 343:399–403

Derode A, Larose E, Campillo M, Fink M (2003) How to estimate the Green's function of a heterogeneous medium between two passive sensors? application to acoustic waves. Appl Phys Lett 83:3054–3056. https://doi.org/10.1063/1.1617373

Durand S, Montagner JP, Roux P, Brenguier F, Nadeau RM, Ricard Y (2011) Passive monitoring of anisotropy change associated with the Parkfield 2004 earthquake. Geophys Res Lett 38:142–154

Gouédard P, Seher T, McGuire JJ, Collins JA, van der Hilst RD (2014) Correction of ocean-bottom seismometer instrumental clock errors using ambient seismic noise. Bull Seismol Soc Am 104:1276–1288. https://doi.org/10.1785/0120130157

Haney MM, Power J, West M, Michaels P (2012) Causal instrument corrections for short-period and broadband seismometers. Seismol Res Lett 83:834–845. https://doi.org/10.1785/0220120031

Hannemann K, Krüger F, Dahm T (2014) Measuring of clock drift rates and static time offsets of ocean bottom stations by means of ambient noise. Geophys J Int 196:1034–1042. https://doi.org/10.1093/gji/ggt434

Lin FC, Ritzwoller MH, Townend J, Bannister S, Savage MK (2007) Ambient noise Rayleigh wave tomography of New Zealand. Geophys J R Astron Soc 170:649–666

Meier U, Shapiro NM, Brenguier F (2010) Detecting seasonal variations in seismic velocities within Los Angeles basin from correlations of ambient seismic noise. Geophys J Int 181:985. https://doi.org/10.1111/j.1365-246X.2010.04550.x

Moschetti MP, Ritzwoller MH, Shapiro NM (2007) Surface wave tomography of the western United States from ambient seismic noise: Rayleigh wave group velocity maps. Geochem Geophys Geosyst 8:Q08010. https://doi.org/10.1029/2007GC001655

Paul A, Campillo M, Margerin L, Larose E, Derode A (2005) Empirical synthesis of time-asymmetrical Green functions from the correlation of coda waves. J Geophys Res Solid Earth 110:B08302. https://doi.org/10.1029/2004JB003521

Prieto GA, Beroza GC (2008) Earthquake ground motion prediction using the ambient seismic field. Geophys Res Lett 35:137–149

Sabra KG, Gerstoft P, Roux P, Kuperman WA, Fehler MC (2005) Extracting time-domain Green's function estimates from ambient seismic noise. Geophys Res Lett 32:L03310. https://doi.org/10.1029/2004GL021862

Sato H (2013) Green's function retrieval from the CCF of random waves and energy conservation for an obstacle of arbitrary shape: noise source distribution on a large surrounding shell. Geophys J Int 193:997–1009. https://doi.org/10.1093/gji/ggt032

Seats KJ, Lawrence JF, Prieto GA (2012) Improved ambient noise correlation functions using Welch's method. Geophys J Int 188:513–523. https://doi.org/10.1111/j.1365-246X.2011.05263.x

Sens-Schönfelder C (2008) Synchronizing seismic networks with ambient noise. Geophys J Int 174:966–970. https://doi.org/10.1111/j.1365-246X.2008.03842.x

Sens-Schönfelder C, Wegler U (2006) Passive image interferometry and seasonal variations of seismic velocities at Merapi Volcano, Indonesia. Geophys Res Lett 33:L21302. https://doi.org/10.1029/2006GL027797

Shapiro NM, Campillo M (2004) Emergence of broadband Rayleigh waves from correlations of the ambient seismic noise. Geophys Res Lett 31:07614. https://doi.org/10.1029/2004gl019491

Shapiro NM, Campillo M, Stehly L, Ritzwoller MH (2005) High-resolution surface-wave tomography from ambient seismic noise. Science 307:1615–1618. https://doi.org/10.1126/science.1108339

Snieder R (2004) Extracting the Green's function from the correlation of coda waves: a derivation based on stationary phase. Phys Rev E. https://doi.org/10.1103/physreve.69.046610

Stehly L, Campillo M, Shapiro NM (2006) A study of the seismic noise from its long-range correlation properties. J Geophys Res Solid Earth 111:B10306. https://doi.org/10.1029/2005JB004237

Stehly L, Campillo M, Shapiro NM (2007) Traveltime measurements from noise correlation: stability and detection of instrumental time-shifts. Geophys J Int 171:223–230. https://doi.org/10.1111/j.1365-246X.2007.03492.x

Weaver RL, Lobkis OI (2001) Ultrasonics without a source: thermal fluctuation correlations at MHz frequencies. Phys Rev Lett 87:134301. https://doi.org/10.1103/PhysRevLett.87.134301

Wegler U, Sens-Schönfelder C (2007) Fault zone monitoring with passive image interferometry. Geophys J Int 168:1029–1033. https://doi.org/10.1111/j.1365-246X.2006.03284.x

Xia Y, Ni S, Zeng X, Xie J, Wang B, Yuan S (2015) Synchronizing intercontinental seismic networks using the 26 s persistent localized microseismic source. Bull Seismol Soc Am 105:2101–2108. https://doi.org/10.1785/0120140252